American Journal of Botany 93(9): 1265–1273. 2006.

INTER-TRACHEID PITTING AND THE HYDRAULIC EFFICIENCY OF CONIFER WOOD: THE ROLE OF TRACHEID ALLOMETRY AND CAVITATION PROTECTION[1]

JARMILA PITTERMANN,[2,5] JOHN S. SPERRY,[3] UWE G. HACKE,[3] JAMES K. WHEELER,[4] AND ELZARD H. SIKKEMA[3]

[2]Department of Integrative Biology, University of California, Berkeley, California 94720 USA; [3]Department of Biology, University of Utah, Salt Lake City, Utah 84112 USA; and [4]Biological Laboratories, Harvard University, Cambridge, Massachusetts 02138 USA

Plant xylem must balance efficient delivery of water to the canopy against protection from air entry into the conduits via air-seeding. We investigated the relationship between tracheid allometry, end wall pitting, safety from air-seeding, and the hydraulic efficiency of conifer wood in order to better understand the trade-offs between effective transport and protection against air entry. Root and stem wood were sampled from conifers belonging to the Pinaceae, Cupressaceae, Podocarpaceae, and Araucariaceae. Hydraulic resistivity of tracheids decreased with increasing tracheid diameter and width, with 64 ± 4% residing in the end wall pitting regardless of tracheid size or phylogenetic affinity. This end-wall percentage was consistent with a near-optimal scaling between tracheid diameter and length that minimized flow resistance for a given tracheid length. There was no evidence that tracheid size and hydraulic efficiency were constrained by the role of the pits in protecting against cavitation by air-seeding. An increase in pit area resistance with safety from cavitation was observed only for species of the northern hemisphere (Pinaceae and Cupressaceae), but this variable was independent of tracheid size, and the increase in pit resistance did not significantly influence tracheid resistance. In contrast to recent work on angiosperm vessels, protection against air-seeding in conifer tracheids appears to be uncoupled from conduit size and conducting efficiency.

Key words: allometry; Araucariaceae; cavitation; conifer; Cupressaceae; Pinaceae; pits; Podocarpacae; resistivity; tracheid.

The transport of water from the root to the canopy occurs at considerable negative pressure in the xylem. This places the transpiration stream under constant threat of air entry, which could potentially nucleate cavitation in the xylem conduits and consequently reduce water transport efficiency to the canopy (Zimmermann, 1983; Tyree and Sperry, 1989; Sperry and Tyree, 1990; Pockman et al., 1995). Stomatal regulation can reduce water loss and lessen the magnitude of the negative xylem pressures, as can a reduction in leaf area (Saliendra et al., 1995; Oren et al., 1999). However, these are not ideal long-term solutions to reducing the threat of cavitation because photosynthetic carbon uptake is significantly impeded (Farquhar and Sharkey, 1982; Dixon et al., 1995; Brodribb et al., 2002). Accordingly, effective water transport must provide an appropriate margin of cavitation safety while presumably optimizing hydraulic conductivity. If the requirement for safety interferes with conductivity, a trade-off will result.

A major cause of cavitation appears to be the leaking of air from embolized conduits through inter-conduit pits (Crombie et al., 1985; Cochard et al., 1992; Jarbeau et al., 1995). If air-tight pits at conduit end walls are necessarily very resistant to water flow and limit the size of the conduit, a trade-off will exist between the mechanism of cavitation and the hydraulic efficiency of the conduit network. Such a link has been postulated for angiosperm vessels; according to the pit area hypothesis, air-tight vessel end walls require limited vessel pit area, which also limits vessel size and hydraulic conductivity (Hacke et al., 2006; Wheeler et al., 2005). The uniformly thin and porous "homogenous" pit membranes of most angiosperms withstand air entry by capillary forces, and so safety from cavitation should be sensitive to the largest membrane pore in the vessel. The greater the vessel pit area, the greater the chances of a large membrane pore, and hence the leakier the end wall is to air. The pit area hypothesis provides a mechanistic explanation for the highly variable but persistent trend of increasing safety from cavitation with increasing flow resistance through the xylem (Pockman and Sperry, 2000; Martinez-Vilalta et al., 2002).

The inter-tracheid pits of conifers are quite different in structure and function from inter-vessel angiosperm pits, and whether their role in cavitation protection limits tracheid size and hydraulic efficiency is unknown. Conifer pits are composed of secondary wall borders arching over the pit membrane, which consists of a dense, disk-like torus suspended within a porous margo region (Siau et al., 1984). In conifer pits, the micrometer-scale margo pores are usually too large to contain an embolus, but are small enough for capillary forces to deflect the pit membrane against the pit border and thus prevent the spread of air from an air-filled tracheid to an adjacent tracheid under negative pressure (Liese and Bauch, 1967; Petty, 1972; Sperry and Tyree, 1990). Cavitation apparently occurs when the torus slips from its sealing position against the aperture, allowing air to enter the functional tracheid (Sperry and Tyree, 1990; Hacke et al., 2004). Do air-tight end walls that promote cavitation safety also compromise conducting efficiency? Modeling studies suggest there is a trade-off at the level of the individual conifer pit (Hacke et al., 2004), but it is not known whether this is true of actual pits and whether a pit-level trade-off influences

[1] Manuscript received 3 October 2005; revision accepted 15 June 2006.

Funding was provided by NSERC (Canada) and NSF DDIG 0308862 (J.P.), and NSF-IBN-0416297 (J.S.S.). The following individuals generously helped with species collections in the U.S. and abroad: R. Oren, T. Dawson, T. Kursar, L. Coley, R. Wheeler, T. Feild, and R. Sage (U.S. and Canada); B. Bohl and the Forfar group (Bahamas); E. Cameron, M. Clearwater, L. Jesson, and D. Kubien (New Zealand); and H. Brinon, B. Perignon, and M. Blanc (New Caledonia).

[5] Author for correspondence (e-mail: pittermann@berkeley.edu)

tracheid size and the overall hydraulic efficiency of the tracheid network.

This paper quantifies the contribution of end wall resistance and pit structure to the hydraulic efficiency of conifer wood and evaluates whether this contribution is linked to protection against cavitation by air-seeding through these end walls. The significance of end wall resistance is mostly a question of the allometry between tracheid diameter and length. The longer tracheids are for a given diameter, the farther apart the end walls are and the less they contribute to the total flow resistance. We evaluate whether constraints on tracheid size and allometry can be causally linked to the role of pitting in cavitation protection.

The results are based on a survey of four phylogenetically distinct conifer families, from which ecologically contrasting species were selected whenever possible. Particularly within the Pinaceae and Cupressaceae, species were sampled from cold and dry to warm and moist environments. All of the conifers we examined are known to have a torus–margo pit structure in earlywood tracheids (Bauch et al., 1972). Recent phylogenetic analyses by Chaw et al. (2000) identify the Pinaceae, Cupressaceae, Podocarpaceae, and Araucariaceae as the dominant conifer clades, of which the first two reside primarily in the northern hemisphere while the Podocarpaceae and Araucariaceae are found in the southern hemisphere. The southern hemisphere conifers are regarded as relicts of the Gondwanan flora and have only recently attracted eco-physiological research (Brodribb and Hill, 1997, 1998, 1999; Feild and Brodribb, 2001).

MATERIALS AND METHODS

Plant material—Table 1 lists the study species and collection sites. We collected both stems and roots whenever possible with a minimal sample size of four segments of either organ for each species. Stem and root segments were longer than 16 cm, with stems measuring approximately 8–10 mm in diameter, while the roots were typically less than 5 mm in diameter. Care was taken to harvest material with a minimum amount of compression wood because its presence may alter the hydraulic properties of the segment (Domec and Gartner, 2002). Samples from all species were wrapped in moist paper towels and plastic bags while transported to our laboratory, but species collected from locations outside of Utah were shipped by overnight express. Samples collected from the Bahamas, New Zealand, and New Caledonia were in transit for approximately 3–7 d due to customs inspection. To test whether or not samples analyzed a week after collection would exhibit significant differences in their hydraulic response, the conductivity and vulnerability to cavitation was measured on stems of *Pinus contorta* either on the day of harvest or following a week at room temperature. The results indicated no significant differences in either the hydraulic conductivity or vulnerability to cavitation in both groups of stems (data not shown).

Tracheid area resistivity (R_{CA})—Our measure of hydraulic efficiency was the resistivity of a tracheid on a cross-sectional area basis, including the walls (R_{CA}). The hydraulic resistivity of a stem or root segment (R) was measured according to the method of Sperry (1993) and calculated as the pressure gradient for a given flow rate. The root and stem samples were prepared by recutting to a length of 142 mm and shaving the ends with a razor blade. The bark was left intact on all stems and roots with the exception of *Pinus monophylla*, for which the bark was removed to prevent the accumulation of excess resin or mucilage. The material remained wet at all times to minimize the entry of air into the exposed xylem.

The segments were mounted on a tubing apparatus where R was measured gravimetrically under a pressure of 5 kPa using filtered water (0.22 μm, E-Pure filtration system, Barnstead International, Dubuque, Iowa, USA). We determined the flow into the segments without a pressure head before and after each gravimetric flow measurement. These background flows were averaged and subtracted from the pressure-induced flow in order to improve accuracy.

The functional xylem area was obtained by perfusing stems with 0.1% basic fuchsin for at least 24 h, sectioning the perfused wood, and measuring the stained area at mid-length under a dissecting scope. The R was converted to a sapwood area basis (R_{Xa}, MPa · s · m^{-2}) by multiplying by the dye-stained area. The R_{Xa} was converted to a tracheid-area basis (R_{CA}, MPa · s · m^{-2}) by multiplying by the tracheid area fraction (tracheid/sapwood area, typically near 0.9) measured on the same cross section.

Partitioning R_{CA} into its structural components—The mean R_{CA} is influenced by the tracheid diameter (D), double wall thickness (T), length (L), the fraction of the tracheid wall area occupied by inter-tracheid pits (F_P), and the resistance of these pits on an area basis (r_P). Using the approach of Wheeler et al. (2005) for angiosperm vessels, we developed an equation for tracheid R_{CA} in terms of these components. The brief derivation below provides the rationale for how we measured certain features.

We assumed that the mean R_{CA} equals the mean lumen resistivity (R_L) plus the mean end wall resistivity (R_W) in series, multiplied by the mean area per tracheid (A_T)

$$R_{CA} = (R_L + R_W)A_T. \quad (1)$$

For a square tracheid

$$A_T = D^2(1 + C)^2, \quad (2)$$

where D is the width of one side and C is the ratio T/D, where T is the double-wall thickness. We assumed that D also determined R_L based on the Hagen–Poiseuille equation for a cylindrical tube

$$R_L = 128\eta/(\pi D^4), \quad (3)$$

where η is the dynamic viscosity (all resistivities were normalized to 20°C). Experiments with vessels have shown that the R_L is accurately modeled by the Hagen–Poiseuille equation (Zwieniecki et al., 2001; Sperry et al., 2005). Although we modeled tracheid transverse shape as square in Eq. 2 and round in Eq. 3, the R_L of a square tube of side D is the same as that of a cylinder with diameter D (Lewis, 1992). The R_W was represented as

$$R_W = r_W/L', \quad (4)$$

where r_W is the end wall resistance and L' is the distance between end walls. We assumed L' was half of the tracheid length ($L' = L/2$) because tracheids will overlap by half on average (Lancashire and Ennos, 2002). The end wall resistance is a function of the area of inter-tracheid pits (A_P) and the pit area resistance (r_P)

$$r_W = 2r_P/A_P, \quad (5)$$

where the factor 2 adjusts the total pit area per tracheid to that of just one of the two end walls. Assuming again a square tracheid shape,

$$A_P = 4DLF_P, \quad (6)$$

where F_P is the fraction of the tracheid wall area occupied by inter-tracheid pits. Combining Eqs. 4–6 and assuming $L' = L/2$ yields

$$R_W = r_P/(DL^2F_P). \quad (7)$$

Substituting Eqs. 7, 3, and 2 into Eq. 1 results in the summary equation for R_{CA}

$$R_{CA} = [128\eta/(\pi D^2) + r_P D/(F_P L^2)](1 + C)^2. \quad (8)$$

Each variable in this equation except for r_P was measured. As described in the following section, variables were measured to be mathematically consistent with this equation for R_{CA}. The equation was solved to yield estimates of r_P. Standard errors of measured mean values for R_{CA} R_L, L, F_P, A_T, and R_W were propagated to calculate means for C, D, r_W, and r_P using standard formulae. For northern hemisphere species, R_L and R_W were not determined on a sample basis and their errors were also calculated.

Tracheid diameter (D) and lumen resistivity (R_L)—The mean tracheid diameter of each xylem sample corresponded to the mean lumen resistivity (R_L) of the sample. Lumen resistivity was calculated by applying the Hagen–Poiseuille equation (Eq. 3) to tracheid lumen diameters.

Hand-cut, transverse sections were made from the xylem in the middle region of the segment used in the R_{CA} measurements described earlier. These

TABLE 1. Study species, family, collection site, figure abbreviation, and pit fractions (F_P) of roots (R) and stems (S) as indicated. Climate data for each species can be found in Pittermann et al. (2006).

Species	Family	Region	Organ	Figure abbreviation	F_P (SE)
Agathis australis (D. Don) Loudon	Araucariaceae	Waikano, North I., New Zealand; 37°25.6′ S, 175°43.2′ E; 100 m a.s.l.; dense forest	R S	aa AA	0.029 (0.007) 0.069 (0.002)
Agathis ovata (C. Moore ex. Veill) Warb	Araucariaceae	New Caledonia, Provence Sud; 22°02′ S, 166°28′ E; 750 m a.s.l.; open shrubland	S	AO	0.046 (0.007)
*Araucaria columnaris** (J.R. Forst) Hooker	Araucariaceae	New Caledonia, Provence Sud; 22°S, 166° E; 120 m a.s.l.; open woodland	S	—	—
Araucaria laubenfelsii Corbasson	Araucariaceae	New Caledonia, Provence Sud; 22°05′ S, 166°26′ E; 120 m a.s.l.; open maquis	S	AL	0.041 (0.004)
Juniperus osteosperma (Torrey) Little	Cupressaceae	St. George, Utah; 37°04′ N, 113°58′ W; 840 m a.s.l.; pinyon-juniper woodland	R S	co CO	0.2 (0.01) 0.114 (0.011)
Juniperus scopulorum Sargent	Cupressaceae	Uinta Mountains, Utah; 40°3′ N, 111°37′ W; 2500 m a.s.l.; juniper woodland	S	CS	0.11 (0.004)
Sequoia sempervirens (D. Don) Endlicher	Cupressaceae	Sonoma, California; 38°53′ N, 123°25′ W; 355 m a.s.l.; coastal forest	R S	cq CQ	0.135 (0.014) 0.084 (0.011)
Taxodium distichum (Linnaeus) Richard	Cupressaceae	Durham, North Carolina; 35°52′ N, 79°59′ W; 130 m a.s.l.; swamp forest	R S S	ct CT PA	0.086 (0.01) 0.092 (0.011) 0.108 (0.007)
Abies lasiocarpa (Hooker) Nuttall	Pinaceae	Brighton, Utah; 40°46′ N, 11°35′ W; 2825 m a.s.l.; subalpine forest	R S	pa PA	0.112 (0.011) 0.108 (0.007)
Picea engelmanii Parry ex Englemann	Pinaceae	Uinta Mountains, Utah; 40°4′ N, 111°2′ W; 2850 m a.s.l.; subalpine forest	R S	pe PE	0.089 (0.008) 0.075 (0.007)
Picea mariana (Miller) Britton Sterns, & Poggenburg	Pinaceae	Fairbanks, Alaska; 64°49′ N, 147°45′ W; 200 m a.s.l.; open woodland Bettles, Alaska; 66°90′ N, 151°58′ W; elevation unknown; boreal forest	R S	pr PR	0.111 (0.014) 0.071 (0.012)
Pinus caribaea Morelet	Pinaceae	Andros I., Bahamas; 24°43′ N, 77°47′ W; 10 m a.s.l.; pine forest	R S	pc PC	0.086 (0.018) 0.077 (0.013)
Pinus contorta Douglas ex Loudon	Pinaceae	Uinta Mountains, Utah; 40°3′ N, 111°37′ W; 2500 m a.s.l.; mid-montane forest	R S	pt PT	0.14 (0.014) 0.113 (0.011)
Pinus monophylla Torrey & Fremont	Pinaceae	St. George, Utah; 37°104′ S, 113°58′ W; 840 m a.s.l.; pinyon-juniper woodland	R S	pm PM	0.186 (0.021) 0.088 (0.007)
Dacrydium cupressinum Solander ex G. Forst	Podocarpaceae	Waikatere, North Island, New Zealand; 37°25.6′ S, 175°43.9′ E; 300 m a.s.l.; dense forest	R S	od OD	0.06 (0.004) 0.043 (0.005)
Phyllocladus trichomanoides D. Don in Lambert	Podocarpaceae	Waikatere, North Island, New Zealand; 37°25.6′ S, 175°43.9′ E; 300 m a.s.l.; dense forest	S	OH	0.03 (0.003)
Podocarpus cunninghamii Colenso	Podocarpaceae	Wellington, New Zealand; 38°53.9′ S, 175°25′ E; 50 m a.s.l.; open woodland	S	OC	0.034 (0.003)
Prumnopytis ferruginea (G. Benn ex D. Don) de Laub.	Podocarpaceae	Waikatere, North Island, New Zealand; 37°25.6′ S, 175°43.9′ E; 300 m a.s.l.; dense forest	R S	op OP	0.054 (0.009) 0.032 (0.008)
Retrophyllum minor Carriere	Podocarpaceae	New Caledonia, Provence Sud; 22°18.6′ S, 166°58′ E; 150 m a.s.l.; open woodland	S	OR	0.083 (0.007)

* Species for which anatomy data were not collected.

sections were stained in toluidine blue for 3 min, rinsed in distilled water, and mounted on a glass slide with glycerin. We photographed the outer 3–4 growth rings of the sections under 200× magnification with a Nikon digital camera mounted on a Nikon Eclipse E600 microscope (Model RT KE, Diagnostic Instruments, Salt Lake City, Utah, USA). Tracheid lumen areas were measured using image analysis software (ImagePro, Media Cybernetics, Carlsbad, California, USA). A minimum of 3–4 radial files of tracheids were measured in 3–6 different sectors of the cross section, depending on the diameter of the root or stem segment. The area containing the measured tracheids, including wall area, was also determined. On average, between 400 and 800 tracheids were measured per root or stem segment.

The tracheid lumen areas were converted to diameters (D) and the individual lumen resistivity (R_L) estimated according to Eq. 3. The sum of the lumen resistivities was divided by the number of tracheids measured to yield the mean R_L of the sector. The segment R_L was the mean of all sectors per segment, and the species R_L was the mean of a minimum of four segments. The mean tracheid diameter (D) was obtained by solving Eq. 3 for D from the species mean R_L.

Thickness-to-span ratio (C) and tracheid transverse area (A_T)—The mean thickness-to-span ratio (C) was determined by solving Eq. 2 for C from D and the mean area per tracheid (A_T) measured on cross sections of xylem samples. The thickness-to-span ratio is important for the mechanical strength of wood in terms of hydraulic transport as well as canopy support, and we emphasize its measurement and significance in a related paper (Pittermann et al., 2006).

End-wall resistivity (R_W) and tracheid resistivity (R_C)—The end-wall resistivity (R_W) was estimated by solving Eq. 1 after measuring R_{CA}, R_L, and A_T. Tracheid resistivity (R_C) was the tracheid area resistivity (R_{CA}) divided by the tracheid area (A_T) and is also given by the sum of $R_L + R_W$.

Tracheid length (L) and inter-tracheid pit anatomy—Pit features and tracheid length were measured on individual tracheids obtained from wood macerations. Small samples of root and stem xylem were cleaned of their periderm and pith and placed in a 1:1 solution of 80%+ glacial acetic acid and 30% hydrogen peroxide overnight at 60°C (Mauseth and Fujii, 1994). The

digested samples were then rinsed in distilled water, stained with toluidine blue for 3–5 min, and mounted on a glass slide with glycerin. Digital photos of whole tracheids were obtained at 20× magnification, and tracheid lengths were measured on at least 50 tracheids using Image Pro software (as described earlier).

The pit area per total tracheid wall area (F_P) was measured on photos of individual tracheids taken at 200× magnification, with at least half of the tracheid in the photo. Pits were confined to radial walls, so only the radial walls were photographed. The total pit area (= membrane area) per area of one longitudinal half of one radial wall was measured. This fraction was divided by two (to account for the unpitted tangential walls) to estimate the total pit area per tracheid wall area. Species mean F_P was calculated from measurements on at least 15 tracheids per species. On the same material we measured the areas of the pit aperture and membrane at 400× magnification. These areas were converted to equivalent circle diameters for the aperture and membrane.

Vulnerability curves and cavitation pressure—We used the centrifuge method to measure the species' vulnerability to water-stress-induced cavitation at progressively more negative xylem pressures (Pockman et al., 1995; Alder et al., 1997). The same root and stem segments from which R_{CA} was obtained were used to generate the vulnerability curves.

Hydraulic conductivity ($K = 1/R$) of the segments at each xylem pressure (P_x) was measured in the laboratory using the Sperry method (Sperry, 1993) as described. We did not flush the stems to remove native emboli to obtain maximum K because in preliminary measurements the conductivity consistently decreased slightly following the flush, meaning there was no detectable native embolism (Mayr et al., 2002; Pittermann and Sperry, 2003).

Following the native conductivity measurement (K_{native}), the segments were spun in a custom-built rotor to increasingly negative xylem pressures (Pockman et al., 1995; Alder et al., 1997). At each xylem pressure, the K was measured to assess the loss in conductivity due to cavitation, and the percentage of loss of conductivity (PLC) was calculated according to $PLC = 100 \times (1 - K/K_{native})$. The PLC vs. xylem pressure data were fit with a Weibull function to calculate the xylem pressure at which the segment showed 50% loss of conductivity (P_{50}). The P_{50} is a convenient representation of the range of cavitation pressure for a sample and has been used extensively to compare the cavitation resistance across species (Hacke and Sperry, 2001; Hacke et al., 2001; Wheeler et al., 2005). For the usually sigmoidal vulnerability curves of conifer material, the P_{50} is very similar to the mean cavitation pressure used to represent cavitation vulnerability in other studies (Hacke et al., 2006).

RESULTS

The R_{CA} ranged over 130-fold from 58 MPa · s · m^{-2} for the large tracheids of *Pinus caribea* roots to 7700 in the small tracheids of *Juniperus osteosperma* stems (Fig. 1, Appendices S1–S3; see Supplemental Data accompanying the online version of this article; these appendices present the data from Figs. 1–7 in tables). The R_{CA} increased with decreasing tracheid diameter ($r^2 = 0.71$) and shorter length ($r^2 = 0.48$; Fig. 1). The variation in R_{CA} was nearly equally divided between lumen (R_L) and end-wall (R_W) components (Fig. 2), with R_W averaging 64 ± 4% of R_C across all tracheid sizes. Hence, we observed a consistently significant end wall limitation to hydraulic efficiency of conifer xylem, and it was independent of tracheid size.

The proportionality between R_L and R_W was associated with proportionality between tracheid diameter and length (Fig. 3). This is because R_L is a function of D (Eq. 3) and R_W is a function of L (Eq. 7). Inspection of Eq. 8 reveals that, all else being equal, there is an optimal diameter for a given tracheid length that will minimize the R_{CA} (Lancashire and Ennos, 2002). A diameter that is too small makes the lumen resistivity increase (first term in Eq. 8, equivalent to R_L on lumen area basis), and a diameter that is too large makes the end wall resistivity increase (second term in Eq. 8, equivalent to R_W on a lumen area basis). Setting the derivative of Eq. 8 with respect to D equal to zero allowed the optimal D (D_{opt}) to be predicted, all else being constant (Lancashire and Ennos, 2002)

$$D_{opt} = [256F_P\eta/(r_P\pi)]^{1/3}L^{2/3}. \quad (9)$$

Actual diameters averaged within 7% of D_{opt}, and R_{CA} averaged within 11% of the minimum (Fig. 4). At D_{opt}, end wall resistivity (R_W) accounts for 67% of R_C, which was close to the observed 64 ± 4% average (Fig. 2). The observed D vs.

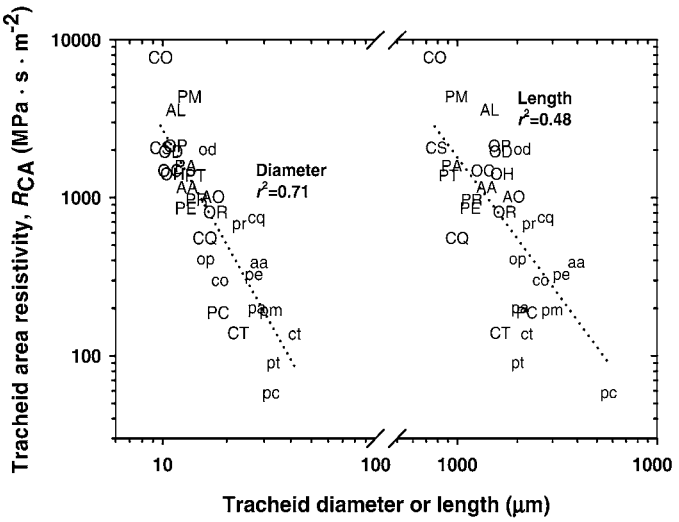

Fig. 1. Tracheid area resistivity (R_{CA}) plotted as a function of tracheid diameter, D, or tracheid length, L (SE averaged 24% of R_{CA}, 7% of D, and 3% of L). Across all species measured, the roots (lowercase letters) typically had wider and longer tracheids than stems (uppercase letters correspond to species in Table 1; see also Appendix S1 accompanying the online version of this article).

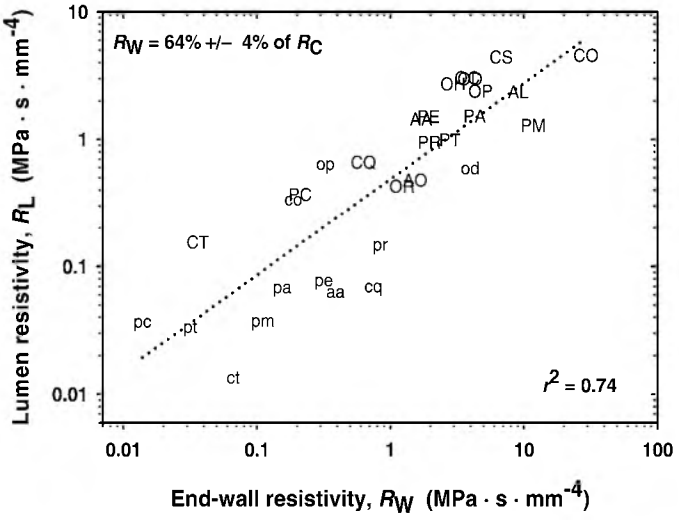

Fig. 2. Lumen resistivity (R_L) plotted as a function of end wall resistivity (R_W) for all species measured (see Table 1 for species abbreviations; lowercase letters correspond to roots; uppercase letters correspond to stems). Values are expressed on a mean tracheid area basis, with R_W contributing approximately 64% to the total tracheid resistivity (R_C). The SE averaged 14% of R_L and 40% of R_W (see also Supplemental Appendix 1 with the online version of this article).

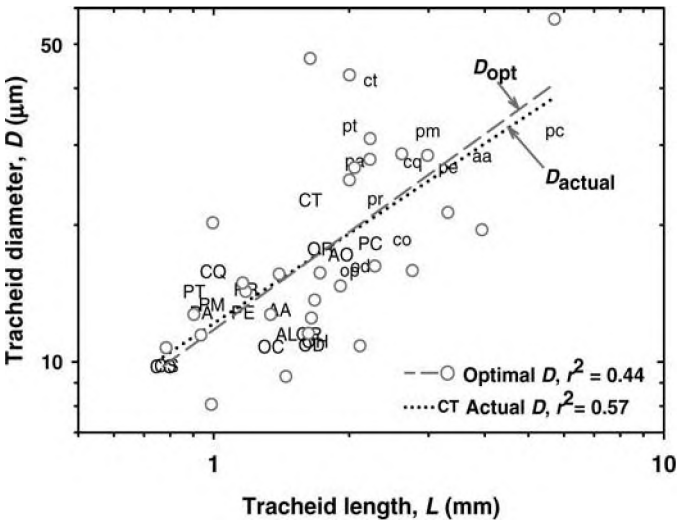

Fig. 3. Tracheid diameter, D, plotted as a function of tracheid length, L, for actual data (species abbreviations [see Table 1 for species abbreviations: lowercase letters correspond to roots; uppercase letters correspond to stems] and dotted regression) and for the optimal tracheid diameter, D_{opt}, as a function of L (open circles and dashed regression, D_{opt} calculated from Eq. 9; see also Appendix S1 with the online version of this article).

L allometry appeared to optimize hydraulic efficiency within constraints on L, F_P, and r_P (Fig. 3; compare dashed optimal regression with dotted data regression).

Vulnerability curves allowed us to assess whether constraints on L, F_P, and r_P could be causally related to protection against cavitation by air-seeding. We generated a total of 30 vulnerability curves for stems and roots (whenever it was possible to collect roots) of each species; the extremes within each family are shown in Fig. 5. We observed a wide range of vulnerability to cavitation across families, between species, and between the roots and stems of a species; *Taxodium distichum* roots (P_{50} of −0.8 MPa) were the most vulnerable, and *J. osteosperma* stems (P_{50} of −7.8 MPa) were the most resistant. Among the five conifer families examined, species of Araucariaceae had the least amount of variation in cavitation resistance.

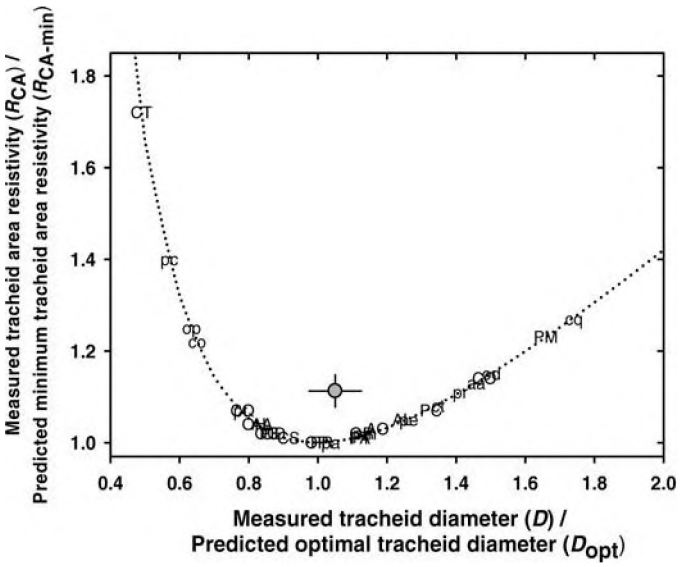

Fig. 4. The ratio of measured R_{CA} relative to theoretical minimum $R_{CA\text{-}min}$ plotted as a function of the ratio of the actual to the optimal diameter (D/D_{opt}). The D_{opt} was determined from Eq. 9, the $R_{CA\text{-}min}$ was calculated from Eq. 8 using D_{opt} for D. The mean R_{CA} was within 11% of $R_{CA\text{-}min}$, and the mean D was within 7% of D_{opt} (grey circle; see also Appendix S2 with the online version of this article). See Table 1 for species abbreviations; lowercase letters correspond to roots; uppercase letters correspond to stems.

Based on the pooled data set, there was no evidence that the wide variation in cavitation vulnerability was related to the r_P of the pits that were presumably setting the air-seeding pressure. Our resolution of r_P was limited, with a standard error averaging 20% of the mean, owing to the number of calculations required to estimate it from measured parameters. Within this capability, however, we found no trade-off between increasing r_P and increasingly negative P_{50} across the full data set, nor was the r_P variation obviously related to the organs sampled (Fig. 6A). The r_P also did not differ between northern (6 ± 6.2 MPa · s · m^{-1}) and southern (5.4 ± 4.4 MPa · s · m^{-1}) hemisphere species.

Within just the northern hemisphere species, however, there was an increase in r_P with P_{50} ($r^2 = 0.46$; Fig. 6A insert). This trade-off was also seen within the Pinaceae ($r^2 = 0.56$) and the Cupressaceae ($r^2 = 0.51$). Separating the southern hemisphere species by family (Podocarpaceae and Araucariaceae) did not result in any r_P vs. P_{50} relationship.

We found no evidence linking total tracheid pit area (A_P) and vulnerability to cavitation (Fig. 6B), which according to the pit area hypothesis determines cavitation safety for the homogenous pits (no torus–margo) of angiosperm vessels (Wheeler et al., 2005). Generally, roots had a greater A_P for a given P_{50} than stems. When stem tracheids alone were considered, a weak relationship was evident ($r^2 = 0.34$; Fig. 6B dotted regression). However, this trend was probably not the result of a direct causal link between pit area and vulnerability because it was not observed in root tracheids. It was not surprising that conifers should differ from angiosperms in this regard given the fundamentally different mechanism of their torus–margo pit functioning.

The fraction of the tracheid wall area that is pitted (F_P) was low and varied little across the data set, averaging 0.086 ± 0.008 (Table 1). It also was not correlated with P_{50}. As with r_P, the low pit fraction and consequently low tracheid pit area (A_P) contributed substantially to the end wall hydraulic bottleneck and represents a hydraulic cost, but this cost was essentially flat and not linked to the magnitude of the safety benefit.

Neither the pit aperture nor pit membrane diameter was found to be significantly related to P_{50} (Fig. 7B, C) although there was a slight decrease in the pit aperture/membrane diameter ratio with more negative P_{50} (Fig. 7A). Analyzing the data by hemisphere or family did not change these conclusions. If the P_{50} is related to the ability of the torus to remain sealed across the pit aperture, this ability does not appear to directly limit any aspect of tracheid pit structure that we measured except perhaps a greater aperture/membrane diameter ratio.

The two aspects of pit structure and function that correlated with P_{50} (r_P within northern hemisphere conifers and aperture/membrane diameter ratio) were not in any obvious way causally dependent on tracheid length (L) or diameter. Any constraint on tracheid size therefore appeared to be independent of the mechanism of drought-induced cavitation.

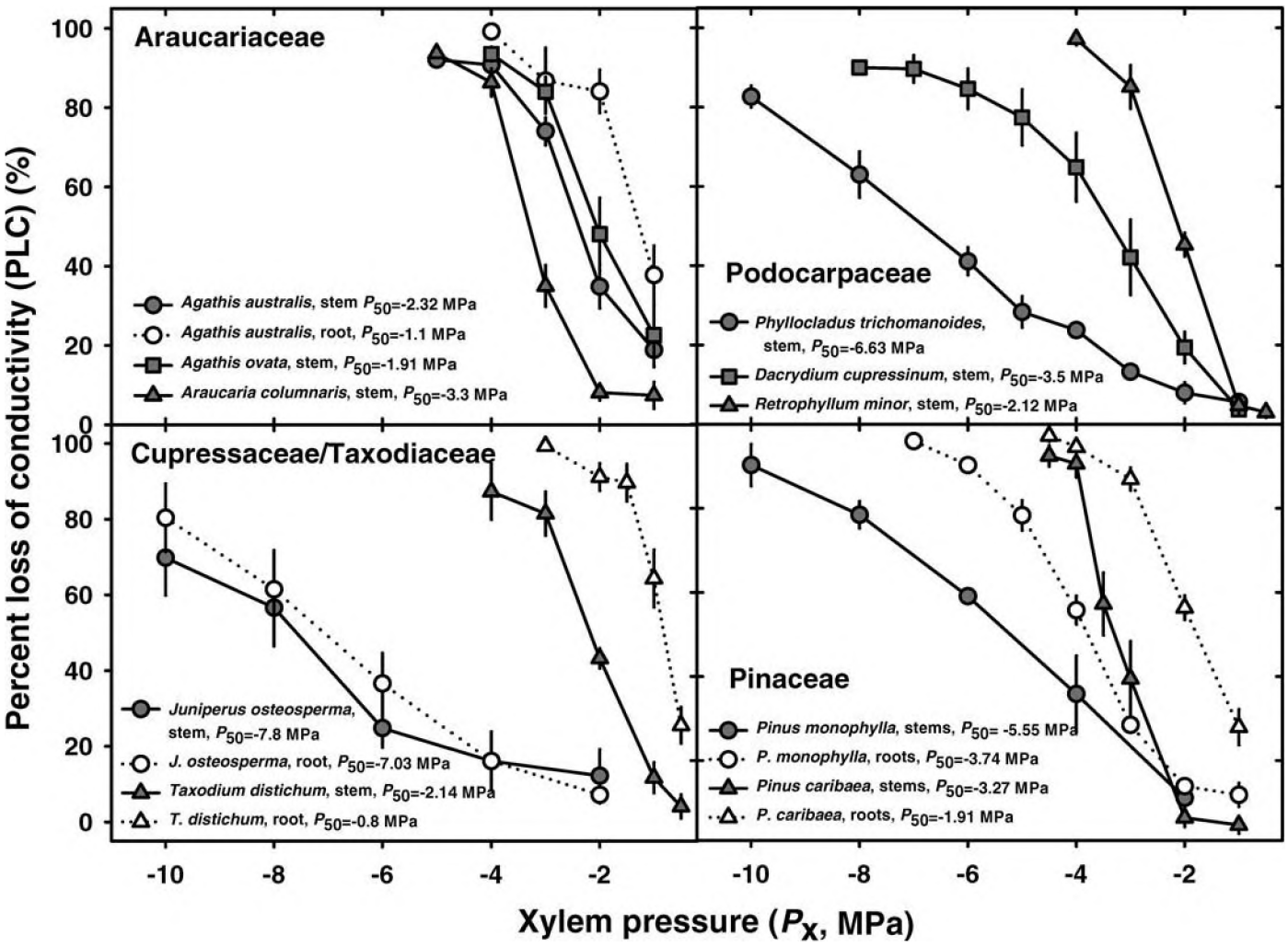

Fig. 5. The percentage loss of conductivity plotted as a function of xylem pressure (vulnerability curve) across selected species in five conifer families. Vulnerability curves were generated for 22 species, but only extreme responses are shown to indicate the degree of variation within each family. Each point represents at least four segments (mean ± SE; see also Appendix S2 accompanying the online version of this article).

DISCUSSION

Our results indicated that the hydraulic efficiency of conifer wood increased with tracheid size (Fig. 1) and was strongly (64 ± 4%) limited by end wall pitting at all sizes (Fig. 2). These results were consistent with near-optimal tracheid diameters for maximizing hydraulic efficiency at a given tracheid length (L), pit fraction (F_P), and pit area resistance (r_P; Figs. 3, 4). However, we observed no evidence that tracheid size and hydraulic efficiency were constrained by the role of inter-tracheid pits in protecting against drought-induced cavitation. Although an increase in r_P with increasing cavitation pressure (P_{50}) was found for northern hemisphere species (Fig. 6A insert), their r_P was not obviously linked to tracheid size, nor was the trend large enough to substantially increase overall xylem resistivity with P_{50}. Similarly, any requirement for smaller pit aperture per membrane diameter to achieve safer xylem (Fig. 7A) does not necessarily dictate smaller tracheid length or diameter.

These conifer results, which show no direct conflict between the cavitation mechanism and tracheid size, directly contrast to those for angiosperms, in which vessel size has been linked to vulnerability to cavitation via the "pit area hypothesis" (Hacke et al., 2006; Wheeler et al., 2005). Unlike the results of these angiosperm surveys, our comparative study of conifer anatomy using similar methodology found no evidence for a link between increasing conduit pit area (A_P) and greater vulnerability to cavitation (Fig. 6B). The air-seeding pressure of a tracheid end wall with torus–margo pit membranes does not drop with the addition of more pits, suggesting a tighter control over the function of individual torus–margo pits than may be possible with the homogenous pit membrane of angiosperms, in which a single large pore is enough to compromise safety (Choat et al., 2003; Hacke et al., 2006).

Given that tracheid pit area does not appear to influence cavitation protection (Fig. 6B), it was surprising that the fraction of the tracheid wall that was pitted (F_P) was so small, averaging only 0.086 ± 0.008 (mean ± SE). The higher the F_P, the larger the optimal lumen diameter (Eq. 9) and the greater the maximum hydraulic efficiency. We speculate that mechanical considerations might limit F_P, because pits are predicted to significantly weaken the tracheid wall (Hacke et al., 2004). It is

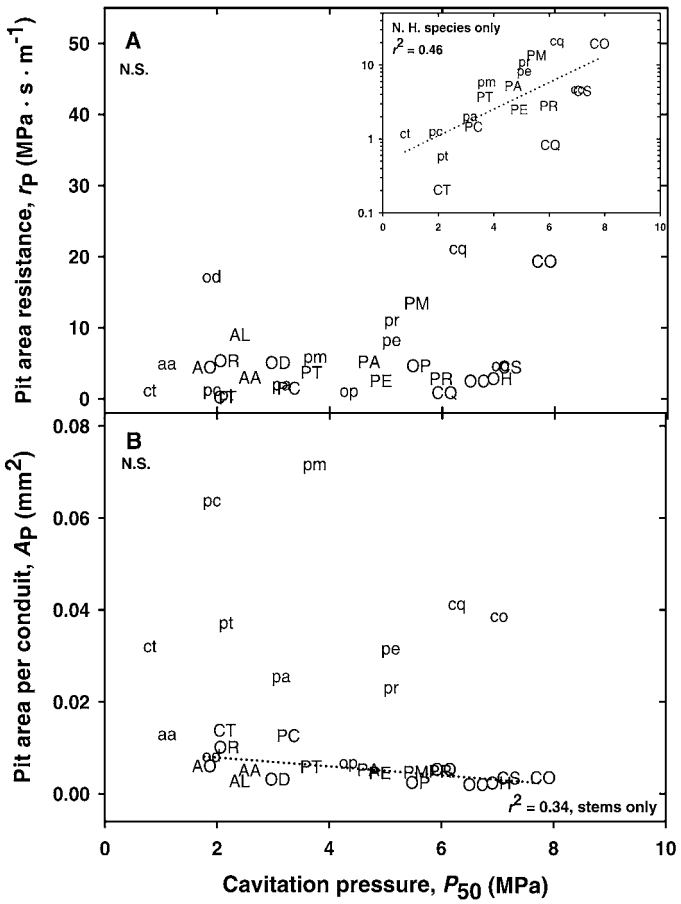

Fig. 6. (A) Pit area resistance (r_P) plotted as a function of cavitation pressure across all species sampled (P_{50}, xylem pressure at which the segment had 50% loss of conductivity). The axes of the inset for northern hemisphere data match those of panel A. The SE averaged 20% of the mean r_P and 12% of the mean P_{50}. (B) Pit area per conduit (A_P) plotted as a function of P_{50}. The SE averaged 14% of the mean A_P. Across the data set, neither one of these end wall features had any relationship to the cavitation pressure, with the exception of r_P for the northern hemisphere species (A, inset; see also Appendix S2 with the online version of this article). See Table 1 for species abbreviations; lowercase letters correspond to roots; uppercase letters correspond to stems. (N.S. = not significant)

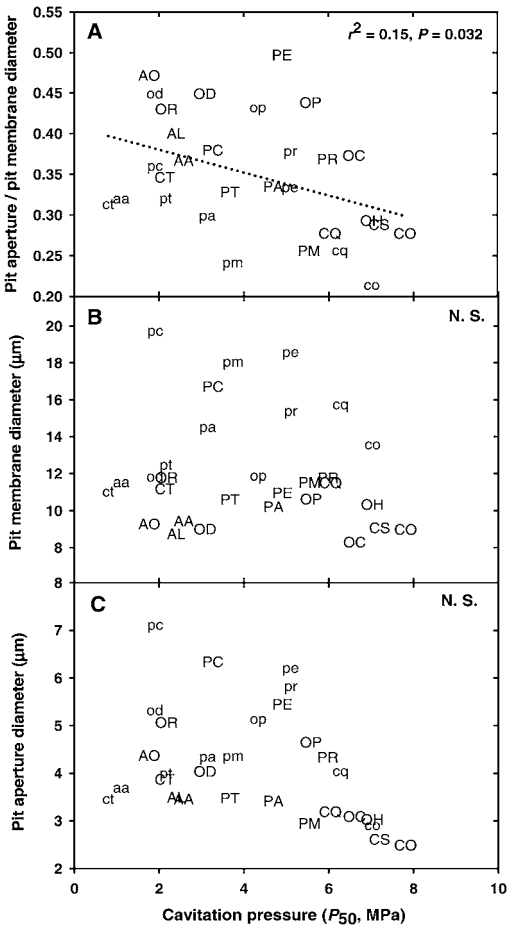

Fig. 7. (A) Pit aperture per pit membrane diameter plotted as a function of cavitation pressure (P_{50}, xylem pressure at which the segment showed 50% loss of conductivity). There was a weak trend toward decreasing aperture to membrane ratios with increasing P_{50}, but no trends are evident between individual pit features across P_{50} (B and C) ($N \geq 50$ pits per species). The SE averaged 1% of the mean pit membrane diameter and 2% of the mean aperture diameter (see also Appendix S3 with the online version of this article). See Table 1 for species abbreviations; lowercase letters correspond to roots; uppercase letters correspond to stems. (N.S. = not significant).

possible that the localization of pits to radial walls may also be an adaptation to minimize their effect on weakening the axis, although we are unaware of any such analysis of this point. A mechanical limit on F_P is consistent with a tendency for F_P to be greater in roots (0.11 ± 0.02), which are less mechanically challenged than stems (0.07 ± 0.01).

Our r_P values (Fig. 6A) are only the second estimates we know of for the torus–margo type of pit. The first was obtained from a physical model of a *Tsuga canadensis* pit and falls in the low end of our range at 0.4 MPa · s · m^{-1} (Lancashire and Ennos, 2002). A mathematical model also predicted rather low r_P values ranging from 0.14 to 0.50 MPa · s · m^{-1} (Hacke et al., 2004). The largest uncertainty in both representations is the margo porosity, which is much more complex to model physically or mathematically than the aperture geometry. When the mathematically modeled resistance of a typical aperture (0.2 MPa · s · m^{-1}; Hacke et al., 2004, fig. 8) is compared to our mean r_P of 5.7 ± 1.3 MPa · s · m^{-1}, the aperture is found to account for <4% of the total r_P. We conclude that the membrane resistance, consisting of the torus and the margo, is the limiting factor for r_P.

The apparently complex relationship between r_P and P_{50} (Fig. 6A) suggests that the air-seeding pressure of the torus–margo valve is not consistently related to the porosity of the margo and hence the r_P. This is somewhat consistent with the mathematical model that predicted a rather weak trade-off (r^2 = 0.19) between pit conductance and air-seed pressure (Hacke et al., 2004). It is intuitive that more margo microfibrils would be needed to hold the torus against a greater air-seeding pressure, thus reducing margo porosity such that the pit r_P should be greater in more cavitation-proof xylem. However, variables other than margo porosity can influence air-seeding pressure of the membrane, including the distance the margo must stretch to reach the aperture and the mechanical properties of the microfibril strands (Hacke et al., 2004). These factors introduce variation in the relationship between margo porosity, and hence r_P, and the pit's air-seeding pressure.

In the case of the southern hemisphere conifers, these types of factors may have completely obscured any relationship between r_P and P_{50}. We observed that aperture shape, in particular, was less circular and more elliptical in the southern hemisphere species. Previous observations have shown that the relative thickness of the torus compared to the margo also differs among families, with the Araucariaceae and Podocarpaceae having thinner tori than members of the Cupressaceae and Pinaceae (Bauch et al., 1972). Perhaps most important in terms of hydraulic function, the margo porosity varies substantially among the four families: the Cupressaceae may exhibit very thick margo regions while the Pinaceae have pits with very porous margos that are clearly differentiated from the torus (Bauch et al., 1972). Limited information is available not only regarding the margo of the Podocarpaceae and Araucariaceae, but also for the overall pit structure of the members of these families. Given the observed phylogenetic effect on r_P, more detailed investigation into the pit structure of the southern hemisphere group may give some insight into the evolutionary, physiological, and/or structural constraints of this unique group of conifers.

The weak correlation between greater cavitation resistance and smaller aperture-to-membrane-diameter ratios (Fig. 7A; Mayr et al., 2002; Burgess et al., 2006) suggests that safer membranes may require a proportionally smaller torus area to bear the distorting pressure difference relative to the supporting membrane and border. In addition, the amount of distortion required to displace the torus could be greater in safer membranes, so a smaller pit aperture may reduce the possibility that the torus will slip from its sealing position to allow air seeding to occur. Because the pit aperture is predicted to contribute <4% to the overall r_P (Hacke et al., 2004), this mechanism of promoting cavitation safety may have little cost in terms of hydraulic resistance.

It is noteworthy that the mean r_P of 5.7 ± 1.3 MPa · s · m^{-1} for torus–margo pits is fully 59 times less than the mean r_P of the homogenous pits of angiosperm vessels (336 ± 81 MPa · s · m^{-1}; Hacke et al., 2006). As emphasized elsewhere (Pittermann et al., 2005), the torus–margo design is much more hydraulically efficient than the angiosperm counterpart, while being just as capable of sealing the tracheid against air entry and cavitation. The low r_P of conifer tracheids is essential to compensate for the short length of tracheids. If tracheids had the high r_P of angiosperms, their end wall resistivity would be >99% of the total tracheid resistivity, and conifer sapwood resistivity would increase by a factor of 38. As it is, low tracheid r_P results in tracheids and vessels having comparable resistivities for the same diameter (Pittermann et al., 2005). Without the evolution of the torus–margo pit, it seems very doubtful that conifers could effectively compete with angiosperms.

If tracheid size is not directly constrained by the need for air-tight end walls to avoid cavitation, then what does limit tracheid size? Lancashire and Ennos (2002) suggested that a single cell is functionally limited in its maximum volume and that this limits the size of the unicellular tracheid. While unicellularity may place an ultimate ceiling on maximum tracheid size, it does not explain the great variation in size across species and organs; in our data set, tracheid length and diameter varied >7.5 times between roots and stems. Instead, there is a species- and organ-specific developmental limit on tracheid length because tracheids show limited intrusive growth, extending only about 10% longer than their fusiform initials (Siau et al., 1984). This is consistent with tracheid diameter being optimized for a constrained tracheid length (Fig. 4). However, the question remains as to what limits fusiform initial length uniquely in different species and organs.

Tracheid size may be limited by mechanical considerations because tracheids supply strength to the wood as well as conducting pathways. Root tracheids may be longer and wider than stem tracheids (Fig. 3) because the wood of small roots does not have to resist the bending and gravitational loads that stem wood does. Tracheids in fern primary xylem can reach over 2 cm in length and 80 μm in diameter (Veres, 1990), and they play little role in mechanical support of the plant, which is held up by non-conducting tissue. In a companion paper on the same data set (Pittermann et al., 2006) we conclude that a limit on tracheid wall thickness results in a potential trade-off between high wood density for strength at the expense of narrow and short tracheids with low conducting efficiency.

Another factor that may influence tracheid size is resistance to freezing-induced cavitation. In both angiosperms and conifers, the smaller the conduit diameter, the greater the resistance to this type of stress (Davis et al., 1999; Sperry and Robson, 2001; Pittermann and Sperry, 2003). We found that conifers with a mean tracheid diameter above ca. 30 μm cavitated significantly by freezing and thawing (Pittermann and Sperry, 2003). However, resistance to freezing may not be the dominant constraint because many conifer species (such as those found in the Podocarpaceae and Araucariaceae) inhabit environments where freezing is extremely rare, and yet their mean tracheid diameters average well below the 30 μm threshold for cavitation by freezing (Fig. 1). This suggests that other considerations, such as mechanical strength, are more important than resistance to freezing-induced cavitation in limiting tracheid width.

The apparent lack of any direct, pit-related hydraulic cost of cavitation resistance in conifers may explain their tendency to have somewhat larger safety margins from cavitation than angiosperms. For example, *Pinus taeda* and *P. ponderosa* tend to close their stomata at a leaf water potential of −2 MPa, yet cavitation in their stem xylem does not begin until xylem pressures drop below −3 MPa (Hacke et al., 2000; Hubbard et al., 2001). Such comfortable safety margins may contribute to the impressive longevity and size of some conifers. In contrast, angiosperms can show very slight margins of safety from cavitation (Pockman and Sperry, 2000; Hacke et al., 2001), consistent with a more direct trade-off between safety and conducting efficiency.

LITERATURE CITED

ALDER, N. N., W. T. POCKMAN, J. S. SPERRY, AND S. NUISMER. 1997. Use of centrifugal force in the study of xylem cavitation. *Journal of Experimental Botany* 48: 665–674.

BAUCH, J. W., W. LIESE, AND R. SCHULTZE. 1972. The morphological variability of the bordered pit membranes in gymnosperms. *Wood Science and Technology* 6: 165–184.

BRODRIBB, T., AND R. S. HILL. 1997. Light response characteristics of a morphologically diverse group of southern hemisphere conifers as measured by chlorophyll fluorescence. *Oecologia* 110: 10–17.

BRODRIBB, T., AND R. S. HILL. 1998. The photosynthetic drought physiology of a diverse group of southern hemisphere conifer species is correlated with minimum seasonal rainfall. *Functional Ecology* 12: 465–471.

BRODRIBB, T., AND R. S. HILL. 1999. The importance of xylem constraints in the distribution of conifer species. *New Phytologist* 143: 365–372.

BRODRIBB, T. J., N. M. HOLBROOK, AND M. V. GUTIERREZ. 2002. Hydraulic and photosynthetic co-ordination in seasonally dry tropical forest trees. *Plant, Cell and Environment* 25: 1435–1444.

BURGESS, S. S. O., J. PITTERMANN, AND T. E. DAWSON. 2006. Hydraulic efficiency and safety of branch xylem increases with height in *Sequoia sempervirens* (D. Don) crowns. *Plant, Cell and Environment* 29: 229–239.

CHAW, S. M., C. L. PARKINSON, Y. CHENG, T. M. VINCENT, AND J. D. PALMER. 2000. Seed plant phylogeny inferred from all three plant genomes: monophyly of extant gymnosperms and origin of Gnetales from conifers. *Proceedings of the National Academy of Sciences, USA* 97: 4086–4091.

CHOAT, B., M. C. BALL, J. LULY, AND J. HOLTUM. 2003. Pit membrane porosity and water stress-induced cavitation in four co-existing dry rainforest tree species. *Plant Physiology* 131: 41–48.

COCHARD, H., P. CRUIZIAT, AND M. T. TYREE. 1992. Use of positive pressures to establish vulnerability curves: further support for the air-seeding hypothesis and implications for pressure-volume analysis. *Plant Physiology* 100: 205–209.

CROMBIE, D. S., M. F. HIPKINS, AND J. A. MILBURN. 1985. Gas penetration of pit membranes in the xylem of *Rhododendron* as the cause of acoustically detectable sap cavitation. *Australian Journal of Plant Physiology* 12: 445–454.

DAVIS, S. D., J. S. SPERRY, AND U. G. HACKE. 1999. The relationship between xylem conduit diameter and cavitation caused by freezing. *American Journal of Botany* 86: 1367–1372.

DIXON, M. L., D. LE THIEC, AND J. P. GARREC. 1995. The growth and gas exchange response of soil-planted Norway spruce (*Picea abies* (L) Karst) and red oak (*Quercus rubra* L) exposed to elevated CO_2 and to naturally occurring drought. *New Phytologist* 129: 265–273.

DOMEC, J.-C., AND B. L. GARTNER. 2002. How do water transport and water storage differ in coniferous earlywood and latewood? *Journal of Experimental Botany* 53: 2369–2379.

FARQUHAR, G. D., AND T. D. SHARKEY. 1982. Stomatal conductance and photosynthesis. *Annual Review of Plant Physiology* 33: 317–345.

FEILD, T. S., AND T. J. BRODRIBB. 2001. Stem water transport and freeze-thaw embolism in conifers and angiosperms in a Tasmanian treeline heath. *Oecologia* 127: 314–320.

HACKE, U. G., AND J. S. SPERRY. 2001. Functional and ecological xylem anatomy. *Perspectives in Plant Ecology, Evolution and Systematics* 4: 97–115.

HACKE, U. G., J. S. SPERRY, B. E. EWERS, D. S. ELLSWORTH, K. V. R. SCHÄFER, AND R. OREN. 2000. Influence of soil porosity on water use in *Pinus taeda*. *Oecologia* 124: 495–505.

HACKE, U. G., J. S. SPERRY, AND J. PITTERMANN. 2004. Analysis of circular bordered pit function. II. Gymnosperm tracheids with torus–margo pit membranes. *American Journal of Botany* 91: 386–400.

HACKE, U. G., J. S. SPERRY, W. P. POCKMAN, S. D. DAVIS, AND K. A. MCCULLOH. 2001. Trends in wood density and structure are linked to prevention of xylem implosion by negative pressure. *Oecologia* 126: 457–461.

HACKE, U. G., J. S. SPERRY, J. K. WHEELER, AND L. CASTRO. 2006. Scaling of angiosperm xylem structure with safety and efficiency. *Tree Physiology* 26: 689–701.

HUBBARD, R. M., M. G. RYAN, V. STILLER, AND J. S. SPERRY. 2001. Stomatal conductance and photosynthesis vary linearly with plant hydraulic conductance in ponderosa pine. *Plant, Cell and Environment* 24: 113–121.

JARBEAU, J. A., F. W. EWERS, AND S. D. DAVIS. 1995. The mechanism of water-stress-induced embolism in two species of chaparral shrubs. *Plant, Cell and Environment* 18: 189–196.

LANCASHIRE, J. R., AND A. R. ENNOS. 2002. Modelling the hydrodynamic resistance of bordered pits. *Journal of Experimental Botany* 53: 1485–1493.

LEWIS, A. M. 1992. Measuring the hydraulic diameter of a pore or conduit. *American Journal of Botany* 79: 1158–1161.

LIESE, W., AND J. BAUCH. 1967. On the closure of bordered pits in conifers. *Wood Science and Technology* 1: 1–13.

MARTINEZ-VILALTA, J., E. PRAT, I. OLIVERAS, AND J. PINOL. 2002. Xylem hydraulic properties of roots and stems of nine Mediterranean woody species. *Oecologia* 133: 19–29.

MAUSETH, J. D., AND T. FUJII. 1994. Resin-casting: a method for investigating apoplastic spaces. *American Journal of Botany* 81: 104–110.

MAYR, S., M. WOLFSCHWENGER, AND H. BAUER. 2002. Winter-drought induced embolism in Norway spruce (*Picea abies*) at the alpine timberline. *Physiologia Plantarum* 115: 74–80.

OREN, R., N. PHILLIPS, B. E. EWERS, D. E. PATAKI, AND J. P. MEGONIGAL. 1999. Sap-flux-scaled transpiration responses to light, vapor pressure deficit, and leaf area reduction in a flooded *Taxodium distichum* forest. *Tree Physiology* 19: 337–347.

PEITY, J. A. 1972. The aspiration of bordered pits in conifer wood. *Proceedings of the Royal Society of London, B, Biological Sciences* 181: 395–406.

PITTERMANN, J., AND J. S. SPERRY. 2003. Tracheid diameter is the key trait determining the extent of freezing-induced embolism in conifers. *Tree Physiology* 23: 907–914.

PITTERMANN, J., J. S. SPERRY, U. G. HACKE, J. K. WHEELER, AND E. H. SIKKEMA. 2005. The torus–margo pit valve makes conifers hydraulically competitive with angiosperms. *Science* 310: 1924.

PITTERMANN, J., J. S. SPERRY, U. G. HACKE, J. K. WHEELER, AND E. H. SIKKEMA. 2006. Mechanical reinforcement against tracheid implosion compromises the hydraulic efficiency of conifer xylem. *Plant, Cell and Environment* 29: 1618–1628.

POCKMAN, W. T., AND J. S. SPERRY. 2000. Vulnerability to xylem cavitation and the distribution of Sonoran Desert vegetation. *American Journal of Botany* 87: 1287–1299.

POCKMAN, W. T., J. S. SPERRY, AND J. W. O'LEARY. 1995. Sustained and significant negative water pressure in xylem. *Nature* 378: 715–716.

SALIENDRA, N. Z., J. S. SPERRY, AND J. P. COMSTOCK. 1995. Influence of leaf water status on stomatal response to humidity, hydraulic conductance, and soil drought in *Betula occidentalis*. *Planta* 196: 357–366.

SIAU, J. F., R. W. DAVIDSON, J. A. MEYER, AND C. SKAAR. 1984. Transport processes in wood. Springer, Berlin, Germany.

SPERRY, J. S. 1993. Winter xylem embolism and spring recovery in *Betula cordifolia, Fagus grandifolia, Abies balsamea,* and *Picea rubens*. *In* M. Borghetti, J. Grace, and A. Raschi [eds.], Water transport in plants under climatic stress, 86–98. Cambridge University Press, Cambridge, UK.

SPERRY, J. S., U. G. HACKE, AND J. W. WHEELER. 2005. Comparative analysis of end wall resistance in xylem conduits. *Plant, Cell and Environment* 28: 456–465.

SPERRY, J. S., AND D. J. ROBSON. 2001. Xylem cavitation and freezing in conifers. *In* F. J. Bigras and S. J. Colombo [eds.], Conifer cold hardiness, 121–136. Kluwer Academic Publishers, Dordrecht, The Netherlands.

SPERRY, J. S., AND M. T. TYREE. 1990. Water-stress-induced xylem embolism in three species of conifers. *Plant, Cell and Environment* 13: 427–436.

TYREE, M. T., AND J. S. SPERRY. 1989. Vulnerability of xylem to cavitation and embolism. *Annual Review of Plant Physiology and Molecular Biology* 40: 19–38.

VERES, J. S. 1990. Xylem anatomy and hydraulic conductance of Costa Rican Blechnum ferns. *American Journal of Botany* 77: 1610–1625.

WHEELER, J. K., J. S. SPERRY, U. G. HACKE, AND N. HOANG. 2005. Inter-vessel pitting and cavitation in woody Rosaceae and other vesselled plants: a basis for a safety versus efficiency trade-off in xylem transport. *Plant, Cell and Environment* 28: 800–812.

ZIMMERMANN, M. H. 1983. Xylem structure and the ascent of sap. Springer-Verlag, Berlin, Germany.

ZWIENIECKI, M., P. MELCHER, AND N. HOLBROOK. 2001. Hydraulic properties of individual xylem vessels in *Fraxinus americana*. *Journal of Experimental Botany* 52: 257–264.